Research Article

Dingquan Song, Bin Wang*, Wencan Tao, Xi Wang, Wei Zhang, Mingfeng Dai, Jinyang Li, and Zhuowan Zhou

Synergistic reinforcement mechanism of basalt fiber/cellulose nanocrystals/polypropylene composites

https://doi.org/10.1515/ntrev-2022-0480
received May 12, 2022; accepted August 25, 2022

Abstract: In this article, we prepared novel basalt fiber (BF)-reinforced polypropylene (PP) composites based on the synergistic reinforcement of cellulose nanocrystals (CNCs). First, we compared the enhancement effect of CNCs and silane coupling agent-modified BFs on PP, showing that the enhancement effect of the former was more significant. Subsequently, to further improve the mechanical properties of the composites, CNCs were introduced into the BF-reinforced PP composite system as the third phase, and the results suggested that their combination with BFs could synergistically strengthen the PP matrix composites. Simultaneously, the study also shows that when the mass percentage of CNCs and BFs are 1 and 30%, respectively, the composite achieves the highest mechanical strength, which is 64.31% higher than that of the PP matrix. The systematic characterization revealed the synergistic enhancement mechanism: on the one hand, CNCs not only promoted the improvement of PP crystallinity by heterogeneous nucleation but also formed a wedge-shaped structure between them and BFs through hydrogen bonding to prevent PP molecular movement; on the other hand, the BFs promote not only the extrusion crystallization of the resin matrix but also the network structure formed by the appropriate content of BFs can realize the rapid transmission of external stress.

*** Corresponding author: Bin Wang,** Key Laboratory of Advanced Technologies of Materials (Ministry of Education), School of Materials Science and Engineering, Southwest Jiaotong University, Chengdu 610031, Sichuan, China, e-mail: jeasonbin@163.com
Dingquan Song, Wencan Tao, Xi Wang, Wei Zhang, Mingfeng Dai, Jinyang Li, Zhuowan Zhou: Key Laboratory of Advanced Technologies of Materials (Ministry of Education), School of Materials Science and Engineering, Southwest Jiaotong University, Chengdu 610031, Sichuan, China

Keywords: basalt fiber-reinforced polypropylene, synergistic enhancement of cellulose nanocrystals, surface modification of silane coupling agent

1 Introduction

Polypropylene (PP) is one of the most widely used resins based on its excellent overall properties, including good processability, superior chemical stability, low relative density, and a wide range of service temperatures [1,2]. However, PP is a nonpolar thermoplastic resin with poor mechanical properties compared to thermosetting epoxy resins [3] or high-performance thermoplastic resins including polyphenylene sulfide, polyamide, and polyether ether ketone [4–6]. Compounding PP with high-strength fibers is an effective means to enhance the mechanical properties of PP [7], and the commonly used reinforcing fibers are carbon fiber [8], basalt fiber (BF) [9], glass fiber [10], *etc*. Among them, carbon fiber is expensive [11], and the all-around performance of glass fiber is poor [12]. Amazingly, BF has a reasonable cost and excellent overall performance, thus receiving extensive attention.

BFs have advantages of excellent shear, heat, and corrosion resistance, easy processing, and low production cost and are naturally degradable. Hence, they exhibit outstanding comprehensive properties [13]. During the preparation of composite materials, surface modification of BFs is often required [14]. Common BFs surface modification methods include silane coupling agent modification, plasma treatment, acidification modification, CVD treatment, *etc*. [15–20]. Among them, most researchers favored silane coupling agent modification due to its simple operation and low cost. For example, Deak *et al*. [21] used KH560 to modify the surface of BFs. They then prepared modified BF-reinforced thermoplastic nylon 6 resin matrix composites. The results showed that the possible hydrogen bonding at the fiber–resin interface

improved the tensile strength of the composites. Liua *et al.* [22] used KH550 to modify the surface of BFs and prepared modified BF-reinforced polylactic acid resin matrix composites. The study revealed the reason for improving the mechanical properties of composites due to the coupling layer bridging interface between the fiber and resin, and the incorporation of BF improved the crystallinity of the resin. However, PP is a nonpolar resin [23]. The coupling layer of BFs only modified by silane coupling agent contains many polar groups, which has a limited effect on improving the mechanical properties of PP-based composites [24]. Besides, the process of modifying with coupling agents is relatively complex and requires modification [25]. The effects of silane coupling agents on the mechanical properties of BF-reinforced poly(butylene terephthalate) composites are stated elsewhere. According to the latest research progress, introducing the third component into fiber-reinforced composites can synergistically enhance the mechanical strength of the composites. Therefore, studying the synergistic reinforcement mechanism of the third component is the key to improving the mechanical properties of BF-reinforced PP composites [26]. Li *et al.* [27] used nanoSiO_2 and BFs to synergistic reinforce epoxy, and the results show that nanoSiO_2 effectively improved the interlaminar shear strength and notch impact strength, thus enhancing the ability to resist external forces of the composites. Hashim *et al.* [28] chose nanosilica and graphene to synergistic reinforce epoxy and found that hybrid nanofiller exhibited a better reinforcement effect in mechanical strength compared to other composite samples prepared with single nanofiller. Szakacs and Meszaros [29] found that BFs can help carbon nanotubes with dispersion in polyamide 6 matrix, thus enhancing the mechanical strength of the composites.

Among various third-component synergistic reinforcing fillers, cellulose nanocrystals (CNCs) are known for their green degradability, environmental friendliness, high modulus, and vast source of raw materials [30,31]. CNCs with high crystallinity can be used as nucleating agents [32] and, at the same time, have an excellent enhancement effect on the mechanical properties of the polymer matrix [33]. Bettaieb *et al.* [34] used CNCs with different aspect ratios to reinforce poly(styrene-*co*-butyl acrylate). They investigated the effect of aspect ratio on rigid continuous networks formed by hydrogen bonding. The results show that a high aspect ratio reduces the threshold of CNCs' content for creating a network and increases the overall stiffness of the network, resulting in a more vital confinement ability for resin movement. Wang *et al.* [35] used CNCs to enhance PLA mechanical strength, and the results showed that 0.1 wt% of CNCs could increase the tensile strength of the composite by 880%.

This article studied BFs and CNCs as the reinforcement and the third component, respectively, and their synergistic reinforcement mechanism for PP composites was studied. This research aims to compare the effect of traditional surface modification using a silane coupling agent and the addition of the third component CNCs on the mechanical properties of BF/PP composites. In addition, the effects of CNC and BF contents on the mechanical properties of the composites were evaluated. The characterization results of the composites suggested that CNC not only improved the crystallinity of PP but also formed a wedge-shaped structure on the surface of BF by hydrogen bonding between it and BF, thereby inhibiting the movement of PP molecular chains. At the same time, an appropriate amount of BFs forms a network that is easy for stress transfer inside the composite, which further promotes the improvement of the performance of the composite. It is precisely based on the synergistic reinforcement derived from CNCs and BFs that the corresponding composite exhibits superior performance than the composite reinforced by either side. The fiber-reinforced composite system jumped out of the traditional coupling agent-based fiber surface modification process. It cleverly used the hydrogen bond between CNC and BF to embed a wedge-shaped structure that prevents the movement of PP molecular chains in the stress conduction network. This study's results will bring new enlightenment to the related research of fiber-reinforced composites.

2 Experimental methods

2.1 Materials

MFB821 PP resin was purchased from Saudi Basic Industries Corporation; 13-3qs chopped BFs (dimeter and length are 13 μm and 3 mm, respectively) were produced in Sichuan Jvyuan Basalt Fiber Technology Corporation; CNCs were provided by Chaozhou SCIENCEK New Material Technology Corporation; γ-aminopropyltriethoxysilane (KH550), γ-(2,3-epoxypropoxy) propyltrimethoxysilane (KH560), and γ-methacryloxypropyltrimethoxysilane (KH570) were purchased from Aladdin Reagent (Shanghai) Corporation; and anhydrous ethanol was purchased from Chengdu Haihong Experimental Instrument Corporation.

2.2 Process of modifying the BFs

Before modification treatment, the BFs were broken up using a small household wall breaker (SG-350F, Beijing Ruibali Trading Corporation) to enhance the dispersibility of the fibers, dried in an oven at 120°C to reduce moisture, and then added to the ethanol solution of the silane coupling agent after cooling down. The coupling agent solution was prepared by adding a certain amount of coupling agent to a glass beaker containing a certain amount of anhydrous ethanol, adding a magnetic stirrer and sealing it with plastic wrap, and then stirring for 10 min using a magnetic stirring device to obtain the desired treatment solution. After the treatment solution was configured, a certain amount of BFs was added into the beaker containing the solution. Then, the beaker was sealed and left for 1 h at room temperature. After that, the solution was filtered, and the BFs gotten from the filtration were dried in an oven at 120°C for 4 h. Finally, the modified BFs were taken out and sealed for storage. As a result, the required modified BFs were obtained. The amount of coupling agent is calculated by the mass ratio between the coupling agent contained in the solution attached to the BF surfaces and the added BFs after the filtration is completed and is labeled according to the mass ratio between the coupling agent and the BFs.

2.3 Process of preparing the composites

BFs, PP and CNCs were manually mixed in certain mass ratio, and then, the composite material masterbatchs are prepared by an internal mixer (XSS-300, Shanghai Sci-Tech, the mixing temperature and rotation speed were 190°C and 60 rad/min, respectively). The masterbatches were further prepared into dumbbell-shaped samples (width is 3.8 mm and thickness is 2 mm) by a mini-injection molding machine (HAAKE MiniJet Pro, Thermo Fisher, Germany; the injection temperature, injection pressure, and mold temperature are 190°C, 750 bar, and 80°C, respectively) for mechanical properties test.

2.4 Mechanical properties and structure characterization

The mechanical properties of the composite specimens were tested using a universal tensile tester (UTM4304X, Sansi Zongheng) with a tensile rate of 20 mm/min.

The chemical changes in samples were characterized by FT-IR spectrum (FT-IR, BRUKER Tensor II, BRUKER, Germany). The wavelength ranges of the specimens we tested were 500–4000 cm^{-1}. Specimens were characterized in tensile section using a scanning electron microscope (SEM, CXS-5TAH, Coxem, Korea). The rheological behaviors of specimens were characterized using a stress-controlled rheometer (DHR-1, TA, USA) with a test temperature of 190°C, a strain value of 1%, and a test range of 0.01–100 rad/s.

The crystalline structure of the specimens was characterized using an X-ray diffractometer (X-Ray Diffractometer, XRD, Empyrean, The Netherlands) with an XRD diffractometer using a copper target, an operating voltage of 40.0 kV, a current of 10.0 mA, a scanning speed of 8°/min, and a scanning range of 5–85°. The crystallinity of the composite specimens was calculated according to the following equation:

$$X_c = \frac{S_c}{S_c + S_a} \times 100\%, \tag{1}$$

where X_c is the crystallinity of PP in the test specimen, S_c is the summation of diffraction peak areas, and S_a is the sum of dispersion peak areas.

The crystallization and melt behaviors of the composites were characterized using a differential scanning calorimeter (DSC, Pyris-1, PerkinElmer, USA) under the test conditions of a nitrogen atmosphere starting from 0°C at a temperature increasing rate of 10°C/min to 200°C, holding for 10 min and then cooling down to 0°C at a temperature decreasing rate of 5°C/min, holding for 10 min, and then following the same temperature change path as before. The crystallinity of the DSC specimens was calculated according to the following equation:

$$X_c = \frac{\Delta H_m}{\Delta H_m^0 \times \varphi} \times 100\%, \tag{2}$$

where φ is the mass fraction of PP in the test specimen, X_c is the crystallinity of PP in the test specimen, ΔH_m is the enthalpy of melting of PP in the test specimens, and ΔH_m^0 is the standard enthalpy of melting of PP, which is 177 J/g [36].

3 Results and discussion

3.1 Comparative enhancement effect of coupling agent and CNCs

The mechanical properties of coupling agent-modified BF-reinforced PP composites and CNC-reinforced PP

composites were compared, and the results are shown in Table 1. From Table 1, it can be seen that raw BFs merely enhance the mechanical strength of PP composites for the hydroxyls group containing the surfaces of BFs. Besides, BFs modified by KH550, KH560, and KH570 had slight improvement in the tensile strength of PP, which indicated that the surface modification of BFs with silane coupling agent had an unsatisfactory even negative enhancement effect on the interfacial binding strength between BFs and nonpolar PP [37]. In sharp contrast, 1 wt% of CNCs increased the tensile strength of PP by 20.24%. Based on this, CNC (1 wt%) was introduced into the BF-reinforced PP (10 wt%) composite and the tensile strength of the composite was further increased to 33.69 MPa, which was 31.80% higher than that of PP and increased by 18.33% compared with BFs/PP composites. The above results show that introducing CNCs as the third component in the BFs/PP composite system has a good reinforcement effect.

SEM characterized the tensile section of each sample, and the results are shown in Figure 1. It can be seen from Figure 1 that a large amount of resin adhered to the surface of the pulled-out fibers of the samples reinforced with CNCs, while less resin attached to the other samples, which indicated that the introduction of 1 wt% of CNCs could effectively improve the interface of the composites, thereby increasing the tensile strength of the sample.

3.2 Optimization of preparation conditions for CNC/BFs synergistically reinforced composites

3.2.1 Effect of CNC amount on mechanical properties of composites

The effect of CNCs amount on the mechanical properties of composites was studied, and the results are shown in Table 2. It is apparent that 0.5 wt% CNC could not enhance the mechanical property of the composites. On the other hand, 1.0 wt% CNC significantly increased the mechanical

Table 1: Comparison of the effects of coupling agent and CNCs on the tensile strength of composites

Type of coupling agent	BFs content (wt%)	Coupling agent amount (coupling amount/BFs%)	CNCs content (wt%)	Tensile strength (MPa)
/	/	0	0	28.02 ± 0.15
/	10	0	0	31.21 ± 0.47
KH550	10	1	0	30.74 ± 1.97
KH560	10	1	0	29.44 ± 0.05
KH570	10	1	0	29.87 ± 0.85
/	0	0	1	33.69 ± 0.14
/	10	0	1	37.23 ± 0.29

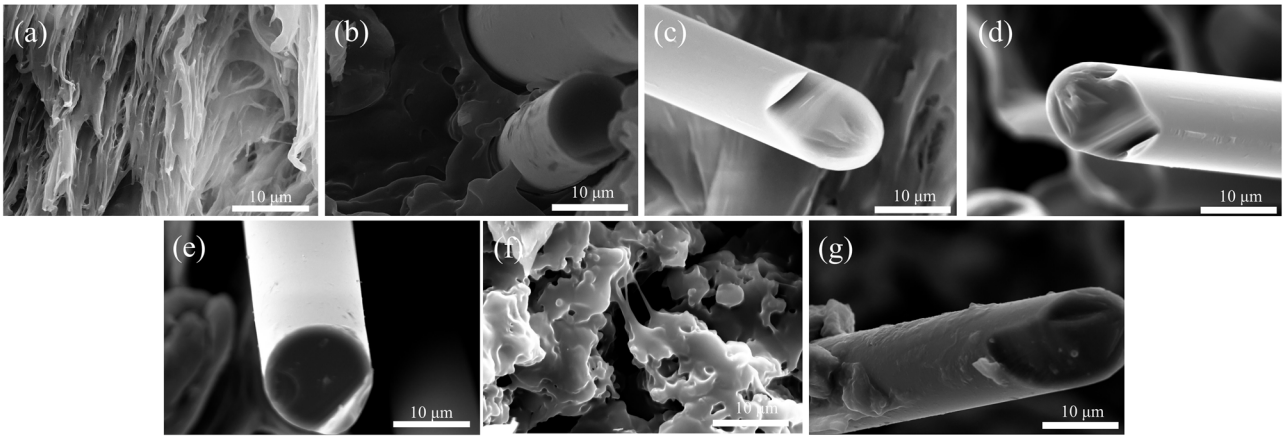

Figure 1: SEM images of tensile cross-sections of composites: (a) PP, (b) PP/10 wt% BFs, (c) PP/10 wt% BFs-1.0 KH550, (d) PP/10 wt% BFs-1.0 KH560, (e) PP/10wt % BFs-1.0 KH570, (f) PP/1 wt% CNCs, and (g) PP/10 wt% BFs/1 wt% CNCs.

Table 2: Tensile strength of composite samples with different CNCs contents when the BF content is 10 wt%

BFs content (wt%)	CNCs content (wt%)	Tensile strength (MPa)
0	1.0	33.69 ± 0.14
10	0.5	33.84 ± 0.11
10	1.0	37.23 ± 0.29
10	1.5	35.36 ± 0.31
10	2.0	35.44 ± 0.49
10	2.5	34.60 ± 0.32

strength of this composite. However, if the amount of CNCs is greater than 1.0 wt%, the mechanical strength of the composite material decreases. Therefore, a small amount of CNC cannot be the best enhancement of the mechanical property. When the amount of CNCs further increases, the enhancement effect is reduced due to the difficulty of uniform dispersion. Therefore, it can be determined that the optimal amount of CNCs is 1.0 wt%.

Table 3: Tensile strength of composites with different BFs content when the CNCs content is 1 wt%

BFs content (wt%)	CNCs content (wt%)	Tensile strength (MPa)
0	1	33.69 ± 0.14
5	1	35.28 ± 0.04
10	1	37.23 ± 0.29
15	1	38.83 ± 0.16
20	1	42.03 ± 0.90
25	1	44.21 ± 0.83
30	1	46.04 ± 1.30
35	1	44.73 ± 1.02
40	1	41.02 ± 2.34
30	0	42.36 ± 0.61

3.2.2 Effect of BF content on the mechanical properties of composites

Table 3 represents the effect of BF content on the mechanical properties of composites that contain 1.0 wt% CNC. With the increase in the fiber content, the composites' mechanical strength gradually increased, reaching the highest (46.04 MPa) when the fiber content was 30 wt %. Compared with pure PP, the mechanical strength is improved by 64.31%, and compared with the composite material without CNCs, it is still improved by 8.69%. However, when the fiber content was further increased, the mechanical strength of the composite showed a decreasing trend.

As mentioned above, the tendency of the composites' mechanical strength to increase first and then decrease is attributed to the fact that the fibers can be well infiltrated by the resin and form a specific network structure when the fiber content is low. The network protects the resin matrix by transferring stress to the fibers when the composite is subjected to external stress. However, when the fiber content exceeds the critical value, the network will be destroyed, and a large number of structure defects will be formed inside the material, resulting in the decline in the mechanical properties of the composite [38]. In this study, the composite achieves the best mechanical strength when the fiber content is 30%. This can be understood as the fiber content is close to or reaching the critical value at this time, which makes the internal network structure of the composite tend to be complete, and can achieve rapid transfer of external stress.

The tensile cross-sections of the 30% BF-reinforced composites containing 1 wt% CNC and without CNC were characterized by SEM, represented in Figure 2. CNC effectively improves the interfacial bonding between the fibers and the matrix in the composite by forming wedge bumps on the surface of extracting fibers, which indicates the

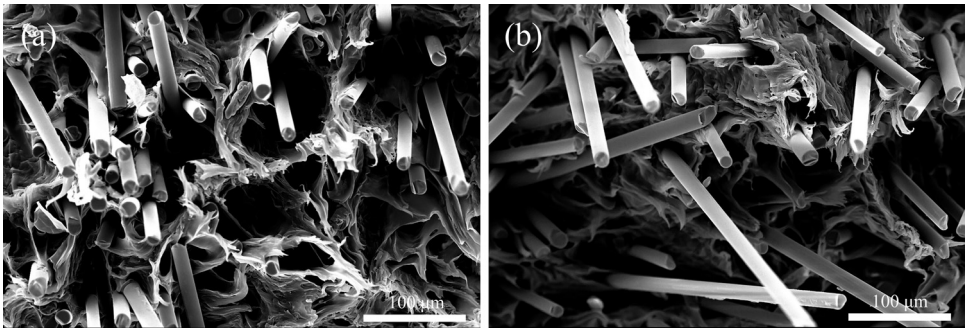

Figure 2: SEM images of tensile cross-sections of composites with and without CNCs when the BF content is 30 wt%: (a) 30 wt% BFs and (b) 30 wt% BFs/1 wt% CNCs.

strong interaction between BFs and CNCs. Therefore, it can be inferred that the introduction of CNCs is beneficial in improving the mechanical strength of the composites.

3.3 Enhancement mechanism study

3.3.1 FT-IR analysis of composites

The surface of BFs and CNCs contains hydroxyl groups [39,40], making it possible to form hydrogen bonds through electrostatic force. By comparing the FT-IR spectra of each sample, it is evidence that after the introduction of BFs and CNCs into the PP matrix, the intensities of the hydroxyl peaks at 3,451 cm^{-1} for BFs and 3,411 cm^{-1} for CNCs are reduced. Their peak positions are red-shifted to 3,288 and 3,312 cm^{-1}, respectively, and the peak shape becomes broader.

In the BFs and CNCs synergistically reinforced PP composites, the hydroxyl group peak is red-shifted to 3,112 cm^{-1}. In addition, the absorbance peak of the CNC incorporated composites corresponding to the C–O bond is red-shifted from 1,020 to 1017 cm^{-1}, which notices the formation of hydrogen bonds between CNCs and BFs through the presence of a large number of hydroxyl groups on the surface. Hydrogen bonding can effectively improve the interfacial bonding of the composite [41], thereby increasing the mechanical strength of the composite (Figure 3).

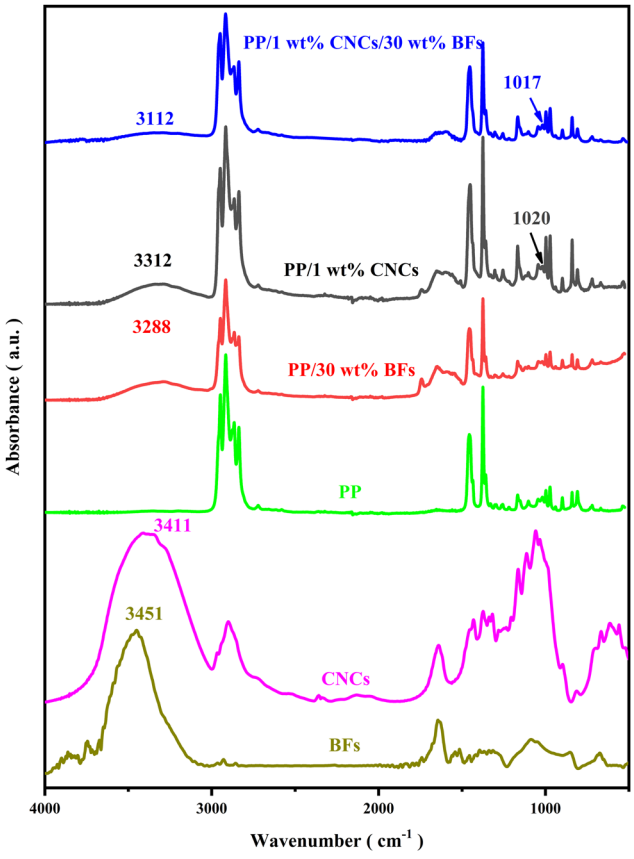

Figure 3: ATR spectra of composites with different component contents.

3.3.2 Effect of CNCs on the crystalline properties of composites

The X-ray diffraction spectra of the composites are shown in Figure 4. Both pure PP and composite materials have diffraction peaks at 2θ = 14.0°, 16.8°, 18.6°, 21.1°, and 21.9°, which correspond to (110), (040), (130), (111), and (131) planes of α-type PP, respectively. In this part, calculate the crystalline structure of PP. For increasing the accuracy of the crystalline of PP, the diffraction peak of BFs was hidden here, and the XRD test results of BFs are shown in the supporting information. Furthermore, Eq. (1) has been used to calculate the crystallinity of PP composites, representing the values in Table 4. The crystallinity of pure PP is about 54.34%, but when CNCs or BFs are introduced, the crystallinity of PP increases to 60.59 and 62.44%, respectively. In particular, the crystallinity of BFs and CNCs synergistically reinforced PP composites exhibited 66.62%, which indicates that the synergistic effect can significantly improve the crystallinity of the PP matrix. Therefore, it notices that BFs and CNCs had a significant influence on the crystallinity of PP. Explaining the above experimental phenomena, the introduction of CNCs to promote the improvement of the crystallinity of the PP matrix is mainly due to the nanoscale heterogeneous nucleation. For BFs, they are primarily attributed to the extrusion-induced crystallization during their coextrusion with the PP matrix. When combining CNCs and BFs synergistically strengthens the PP matrix, the heterogeneous nucleation and coextrusion-induced crystallization coexist, further improving the PP matrix's crystallinity.

Furthermore, the DSC test verified the XRD analysis results represented by Figure 4b and Table 5. DSC and XRD tested the results corresponding to each composite sample. They exhibited different crystallinity but similar laws because the XRD only reflects the components of the surface layer of about 10 nm. In contrast, DSC reflects the enthalpy effect of almost the entire sample. From the XRD and DSC results, it can be seen that the introduction of BFs or CNCs increases the crystallinity of PP, and the PP had the highest crystallinity in the synergistically

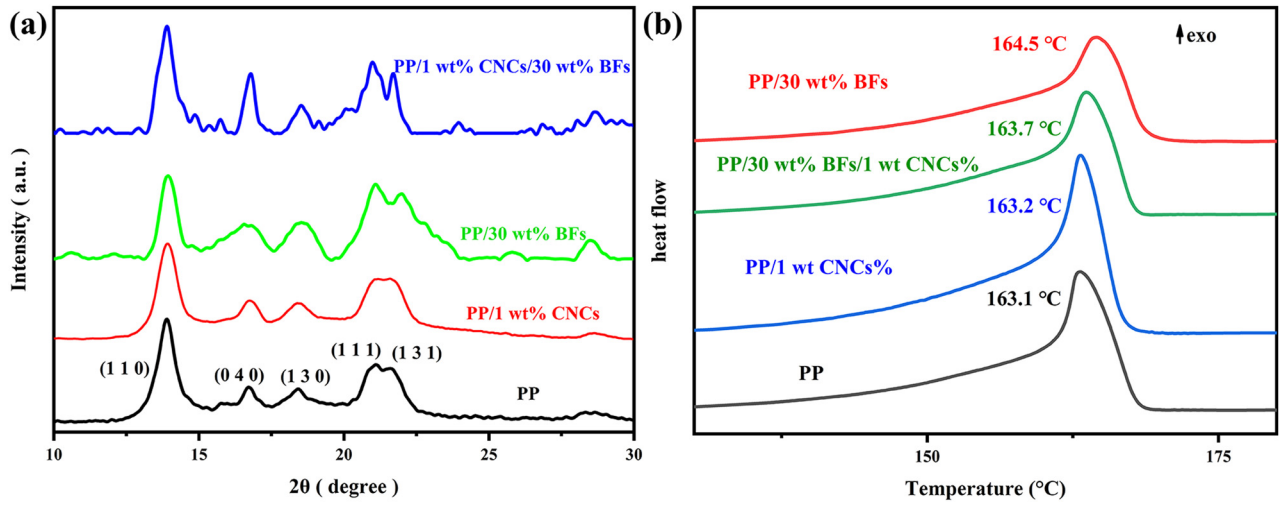

Figure 4: XRD spectra (a) and DCS curves (b) of composites with different component contents.

Table 4: Crystallinity of composites and pure PP

Samples	PP	PP/1 wt % CNCs	PP/30 wt % BFs	PP/1 wt% CNCs/ 30 wt% BFs
X_c (%)	54.34	60.59	62.44	66.62

Table 5: DSC results of composites

BFs content (wt%)	CNCs content (wt%)	T_m (°C)	X_c (%)
0	0.0	163.1	42.66
0	1.0	163.2	53.43
30	1.0	163.7	60.87
30	0.0	164.5	54.38

reinforced composites. However, the melt temperature of the composite is slightly lower than that of BF-reinforced composites, but slightly higher than that of CNC-reinforced composites, which is due to the melt temperature of CNC-reinforced PP composite being lower than that BF-reinforced composite.

3.3.3 Rheological behavior analysis of composites

The rheological behaviors of the composites were evaluated (Figures 5 and 6). The introduction of CNCs can slightly improve the storage modulus (G'), loss modulus (G''), and complex viscosity (η^*) of composites because CNCs with a particular aspect ratio can effectively constrain PP molecular chains; it can also inhibit the interface relaxation behavior. The above effects enhance the deformation resistance of the material and the internal friction between the molecular chains. BFs-reinforced composite is compared with the CNC-reinforced composite, the G', G'', and η^* of the former are greater than those of the latter, indicating that BFs have a more substantial constraining effect on the motion of PP molecular chains. G', G'', and η^* increase further for the composites reinforced by BFs and CNCs synergistically. It is worth noting that the rise in G', G'', and η^* of the composite is not a simple linear sum of the single enhancement changes in each component but is greater than the linear sum, which indicates the synergy between BFs' and CNCs' effect. Under the synergistic effect, the material exhibits stronger resistance to deformation. Based on the FT-IR analysis, it can be seen that this is due to the formation of a large number of hydrogen bonds between CNCs and BFs, effectively improving the composite melt's deformation resistance.

Figure 6 illustrates the Cole–Cole curves of the composites. It can be seen from Figure 6a that the viscous response dominates the material at low shear frequencies. The introduction of CNCs has little effect on the PP, manifested by the high linearity of the corresponding Han curve. When BFs were introduced into PP, the Han curve showed a trend of approaching the diagonal, and the linearity also decreased, indicating that the contribution of elastic response to the increased viscoelasticity of the polymer. For the composites reinforced by BFs and CNCs synergistically, the Han curve is closer to the diagonal, showing a strong interaction between BFs and CNCs. The Cole–Cole curves in Figure 6b show the degree of phase separation in the material melt and the

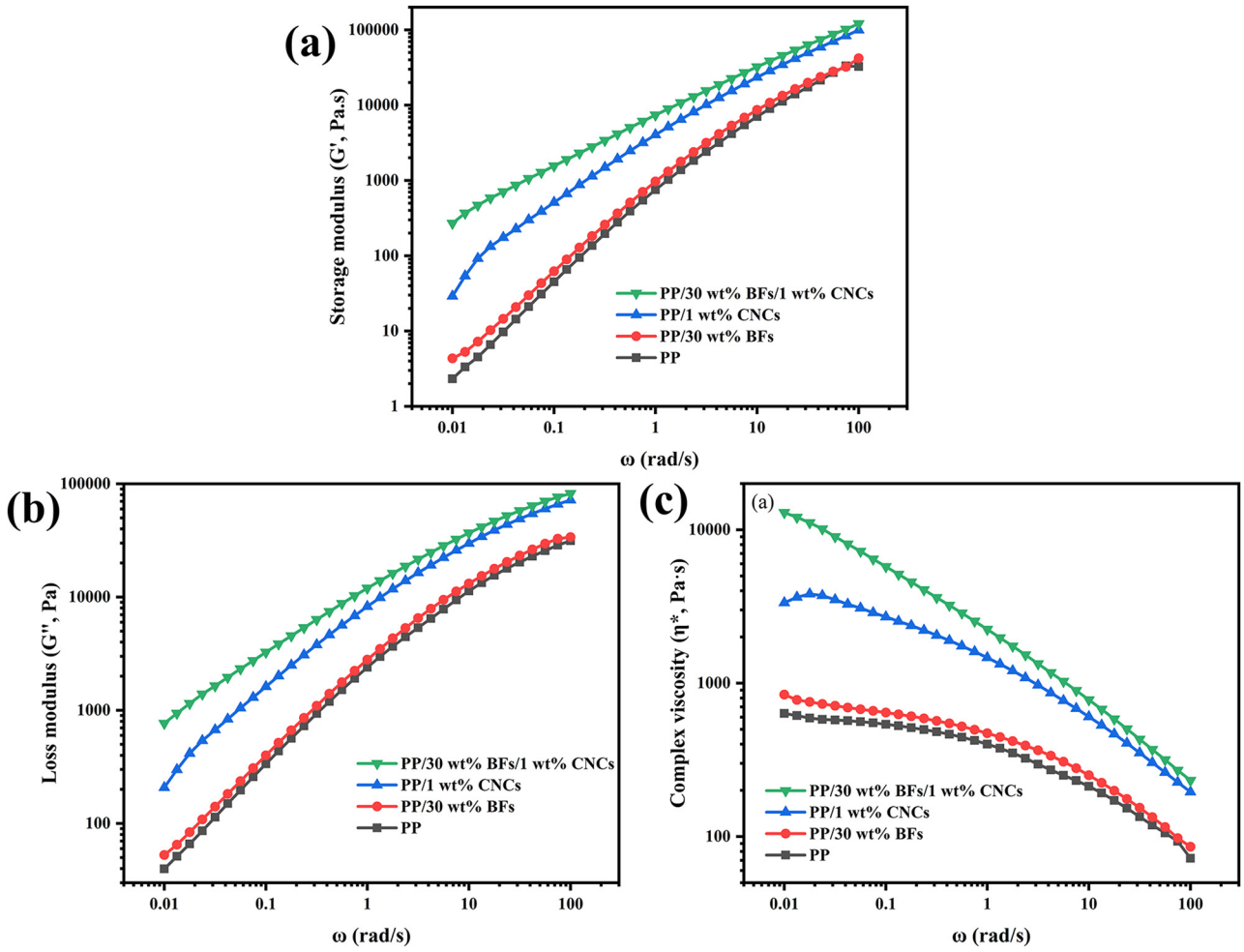

Figure 5: Comparison of storage modulus, loss modulus, and complex viscosity (η^*) of composites with different contents of CNCs and BFs from analyzing rheological behaviors: (a) storage modulus, (b) loss modulus, and (c) complex viscosity (η^*).

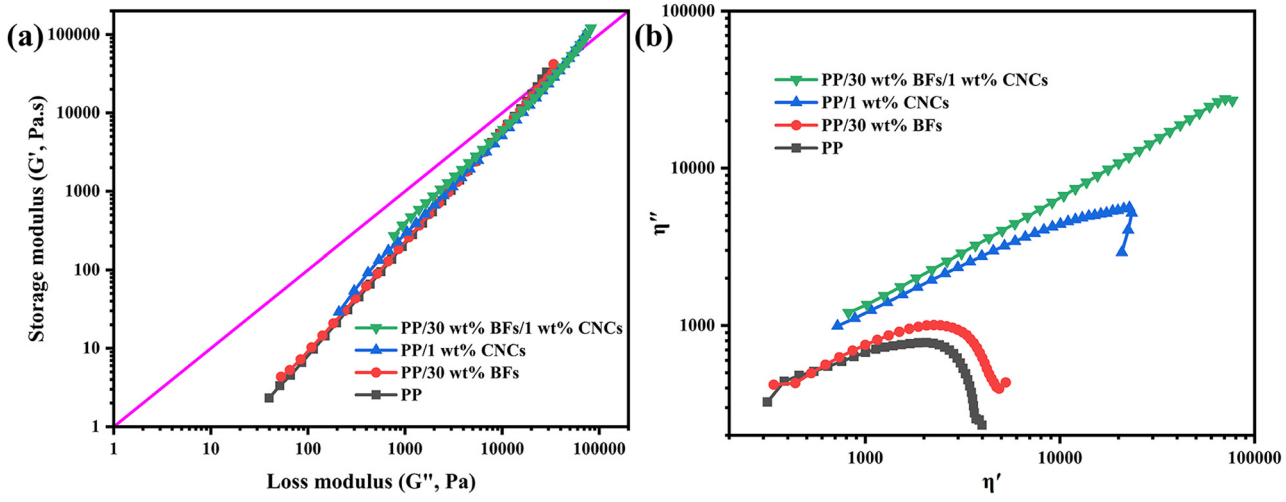

Figure 6: Comparison of Han curves and Cole–Cole curves of composites with different contents of CNCs and BFs from analyzing rheological behaviors: (a) Han curves and (b) Cole–Cole curves.

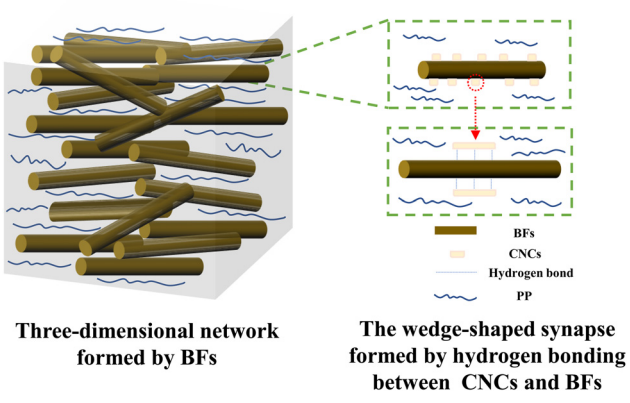

Figure 7: Mechanism diagram of the synergistic enhancement of polypropylene by CNC and basalt fiber.

relaxation state of each phase. The Cole–Cole curve of PP presents an arc in a certain sense, and the curve was still basically an arc after adding CNCs, indicating that the CNCs were uniformly dispersed in the PP melt [42]. However, the two regions appear at high shear frequencies because the relaxation states of CNCs and PP are different, indicating that they are not entirely compatible [43]. The introduction of BFs with a large aspect ratio will dramatically change the material's shape of the Cole–Cole curve of the material, from the circular arc corresponding to pure PP to the straight line. This phenomenon is related to the three-dimensional structure and heterogeneity of the material [44–46]. On this basis, the Cole–Cole curve of the composites reinforced by BFs and CNCs synergistically deformed further, and the curve almost completely transformed into a straight line. These results prove that under the synergistic effect of CNCs and BFs, the three-dimensional network structure in the material tends to be perfect.

Schematic mechanism of the synergistic enhancement of PP by CNCs and BFs can be postulated in Figure 7: first, the introduction of BFs and CNCs into the PP matrix improves the crystallinity of PP to a certain extent; second, an appropriate amount of BFs is introduced into the PP matrix, and they overlap each other to form a three-dimensional network that can conduct external stress in time; and third, CNCs were fixed on the surface of BFs to form a wedge-shaped structure that prevented the movement of PP molecular chains, based on the hydrogen bonding between CNCs and BFs. It is precisely based on the above series of synergistic effects of CNCs and BFs that the composite exhibits excellent mechanical properties.

4 Conclusion

In conclusion, this study proposes a new strategy for preparing high-performance BF-reinforced PP composites. This strategy introduces CNCs as the third phase into the BF-reinforced PP composite system. CNCs enhanced the crystallinity of PP through heterogeneous nucleation. Meanwhile, they formed a wedge-shaped structure with BFs that inhibited the movement of PP molecules. The synergistic enhancement of the above two effects promotes the corresponding composites (the mass percentages of CNCs and BFs are 1 and 30%, respectively) to exhibit excellent mechanical properties.

Funding information: This work was financially supported by the Central University Science and Technology Innovation Project (2682021CX112), Key R&D Program of Sichuan Province (2022YFSY0024), Major Science and Technology Project of Advanced Materials in Sichuan Province (2020ZDZX0016), and the Science and Technology Planning Project of Sichuan Province (2021ZYD0053).

Author contributions: All authors have accepted responsibility for the entire content of this manuscript and approved its submission.

Conflict of interest: The authors state no conflict of interest.

References

[1] Liu WF, Cheng L, Li ST. Review of electrical properties for polypropylene based nanocomposite. Compos Commun. 2018;10:221–5.
[2] Himma NF, Anisah S, Prasetya N, Wenten IG. Advances in preparation, modification, and application of polypropylene membrane. J Polym Eng. 2016;36:329–62.
[3] Liu L, Zhang F, Qi Y, Jian XG, Wang JY. Preparation and properties of high strength and high toughness epoxy resin. Polym Mater Sci Eng. 2019;35:35–9.
[4] Li J, Zhang H, Zhang J, Tang Q, Zhou BH, Xu BM, et al. Research progress on the modification of polyamide. N Chem Mater. 2019;47:29–32.
[5] Dong Y, Yu T, Wang X, Zhang G, Lu J, Zhang M, et al. Improved interfacial shear strength in polyphenylene sulfide/carbon fiber composites via the carboxylic polyphenylene sulfide sizing agent. Compos Sci Technol. 2020;190:108056.
[6] Santiago CC, Yelamanchi B, Diosdado De la Peña JA, Lamb J, Roguski K, Turzyński F, et al. Thermoplastic extrusion additive manufacturing of high-performance carbon fiber PEEK lattices. Crystals. 2021;11:1453.

[7] Shubhra QTH, Alam AKMM, Quaiyyum MA. Mechanical properties of polypropylene composites: a review. J Thermoplast Composite Mater. 2013;26(3):362–91.
[8] Tian H, Yao Y, Liu D, Li Y, Jv R, Xiang G, et al. Enhanced interfacial adhesion and properties of polypropylene/carbon fiber composites by fiber surface oxidation in presence of a compatibilizer. Polym Compos. 2019;40:E654–62.
[9] Ralph C, Lemoine P, Archer E, McIlhagger A. Mechanical properties of short basalt fibre reinforced polypropylene and the effect of fibre sizing on adhesion. Compos Part B-Eng. 2019;176:107260.
[10] He Y, Gong W, Zhang DH, Qin SH. Effect of impregnation time on performance of long glass fiber-reinforced polypropylene composites. J Vinyl Addit Technol. 2018;24(2):174–8.
[11] Dhand V, Mittal G, Rhee KY, Park SJ, Hui D. A short review on basalt fiber reinforced polymer composites. Compos Part B-Eng. 2015;73:166–80.
[12] Deak T, Czigany T. Chemical composition and mechanical properties of basalt and glass fibers: a comparison. Text Res J. 2009;79(7):645–51.
[13] Davies P, Verbouwe W. Evaluation of basalt fibre composites for marine applications. Appl Composite Mater. 2018;25(2):299–308.
[14] Deng T, Ji X, Zhao Y, Cao L, Li S, Hwang S, et al. Interface modification strategy of basalt fiber reinforced resin matrix composites. Prog Chem. 2020;32(9):1307–15.
[15] Chuvashov Y, Jashchenko O, Diduk I, Gulik V. The investigation of fiber surface condition from basalt-like rocks for enhanced industrial applications. J Nat Fibers. 2020;19:2953–62. doi: 10.1080/15440478.2020.1838987.
[16] Quan D, Moloney P, Carolan D, Abourayana H, Ralph C, Ivankovic A, et al. Synergistic toughening and electrical functionalization of an epoxy using MWCNTs and silane-/plasma-activated basalt fibers. J Appl Polym Sci. 2021;138(1):e49605.
[17] Kumar V, Mohan N, Bongale A, Khedkar N. Impact of silane treated basalt fibers and montmorillonite nano-clay on polypropylene composites. Mater Res Exp. 2019;6(12):125325.
[18] Ralph C, Lemoine P, Boyd A, Archer E, McIlhagger A. The effect of fibre sizing on the modification of basalt fibre surface in preparation for bonding to polypropylene. Appl Surf Sci. 2019;475:435–45.
[19] Hao B, Förster T, Mäder E, Ma PC. Modification of basalt fibre using pyrolytic carbon coating for sensing applications. Compos Part A-appl Sci Manuf. 2017;101:123–8.
[20] Chang C, Yue X, Hao B, Xing D, Ma PC. Direct growth of carbon nanotubes on basalt fiber for the application of electromagnetic interference shielding. Carbon. 2020;167:31–9.
[21] Deak T, Czigany T, Tamas P, Nemeth C. Enhancement of interfacial properties of basalt fiber reinforced nylon 6 matrix composites with silane coupling agents. Exp Polym Lett. 2010;4(10):590–8.
[22] Liua S-Q, Yu J-J, Wu G-H, Wang P, Liu MF, Zhang Y, et al. Effect of silane KH550 on interface of basalt fibers (BFs)/poly (lactic acid) (PLA) composites. Ind Textila. 2019;70(5):408–12.
[23] Chen HM, Dong X, Zhao Y, Wang DJ. Recycling and chemical upcycling of waste disposable medical masks. Acta Polym Sin. 2020;51(12):1295–306.
[24] Liu S, Wu G, Yu J, Chen X, Guo J, Zhang X, et al. Surface modification of basalt fiber (BF) for improving compatibilities between BF and poly lactic acid (PLA) matrix. Composite Interfaces. 2019;26(4):275–90.
[25] Arslan C, Dogan M. The effects of silane coupling agents on the mechanical properties of basalt fiber reinforced poly(butylene terephthalate) composites. Compos Part B-Eng. 2018;146:145–54.
[26] Wang CC, Zhao YY, Ge HY, Qian RS. Enhanced mechanical and thermal properties of short carbon fiber reinforced polypropylene composites by graphene oxide. Polym Compos. 2018;39(2):405–13.
[27] Li X, Li GM, Su XH. NanoSiO(2), strengthens and toughens epoxy resin/basalt fiber composites by acting as a nano-mediator. J Polym Eng. 2019;39(1):10–5.
[28] Hashim UR, Jumahat A, Jawaid M. Mechanical properties of hybrid graphene nanoplatelet-nanosilica filled unidirectional basalt fibre composites. Nanomaterials. 2021;11(6):1468.
[29] Szakacs J, Meszaros L. Synergistic effects of carbon nanotubes on the mechanical properties of basalt and carbon fiber-reinforced polyamide 6 hybrid composites. J Thermoplast Composite Mater. 2018;31(4):553–71.
[30] Aziz T, Fan H, Zhang X, Haq F, Ullah A, Ullah R, et al. Advance study of cellulose nanocrystals properties and applications. J Polym Environ. 2020;28(4):1117–28.
[31] Eichhorn SJ, Dufresne A, Aranguren M, Marcovich NE, Capadona JR, Rowan SJ, et al. Review: current international research into cellulose nanofibres and nanocomposites. J Mater Sci. 2010;45(1):1–33.
[32] Osorio DA, Niinivaara E, Jankovic NC, Demir EC, Benkaddour A, Jarvis V, et al. Cellulose nanocrystals influence polyamide 6 crystal structure, spherulite uniformity, and mechanical performance of nanocomposite films. ACS Appl Polym Mater. 2021;3(9):4673–84.
[33] Gao S, Su J, Wang W, Fu J, Wang H. High mechanical performance based on the alignment of cellulose nanocrystal/chitosan composite filaments through continuous coaxial wet spinning. Cellulose. 2021;28(12):7995–8008.
[34] Bettaieb F, Khiari R, Dufresne A, Mhenni MF, Belgacem MN. Mechanical and thermal properties of Posidonia oceanica cellulose nanocrystal reinforced polymer. Carbohydr Polym. 2015;123:99–104.
[35] Wang Z, Yao Z, Zhou J, He M, Jiang Q, Li A, et al. Improvement of polylactic acid film properties through the addition of cellulose nanocrystals isolated from waste cotton cloth. Int J Biol Macromol. 2019;129:878–86.
[36] Li JX, Cheung WL, Jia DM. A study on the heat of fusion of beta-polypropylene. Polymer. 1999;40(5):1219–22.
[37] Czigany T, Deak T, Tamas P. Discontinuous basalt and glass fiber reinforced PP composites from textile prefabricates: effects of interfacial modification on the mechanical performance. Composite Interfaces. 2008;15(7–9):697–707.
[38] Zhou H, Liu H, Wang S, Sun J. Mechanical behaviors of basalt fiber reinforced polypropylene composites. Fiber Reinforced Plastics/Composites. 2014;3:4–7.
[39] Xie Y, Hill CAS, Xiao Z, Militz H, Mai C. Silane coupling agents used for natural fiber/polymer composites: a review. Compos Part A-Appl Sci Manuf. 2010;41(7):806–19.
[40] Kargarzadeh H, Ahmad I, Abdullah I, Dufresne A, Zainudin SY, Sheltami RM. Effects of hydrolysis conditions on the morphology, crystallinity, and thermal stability of cellulose

nanocrystals extracted from kenaf bast fibers. Cellulose. 2012;19(3):855–66.
[41] Nasser J, Lin J, Steinke K, Sodano HA. Enhanced interfacial strength of aramid fiber reinforced composites through adsorbed aramid nanofiber coatings. Compos Sci Technol. 2019;174:125–33.
[42] Gr A, Ak BJMTP. Cole-cole plot of graphene nano filler disseminated glass fiber reinforced polymer composites. Mater Today-Proc. 2021;44:3816–22.
[43] Zanjanijam AR, Hakim S, Azizi H. Morphological, dynamic mechanical, rheological and impact strength properties of the PP/PVB blends: the effect of waste PVB as a toughener. Rsc Adv. 2016;6(50):44673–86.
[44] Yuan Z, Lu-min Z, Gan-ce DAI. Correlation between thermal properties and rheological behavior of graphite filled polypropylene. Polym Mater Sci Eng. 2009;25(4):74–6.
[45] Stanciu MD, Teodorescu Draghicescu H, Tamas F, Terciu OM. Mechanical and rheological behaviour of composites reinforced with natural fibres. Polymers. 2020;12(6):1402.
[46] Wang LL, Dong X, Liu X-G, Xin Q, Huang MM. Microstructure and rheological properties of polyurethane and its composites. Acta Polym Sin. 2013;3:367–76.